# Comparisons of electron energy deposition derived from observations of lower thermospheric nitric oxide and from X-ray bremsstrahlung measurements

C. Sætre,[1] C. A. Barth,[2] J. Stadsnes,[1] N. Østgaard,[1] S. M. Bailey,[3] D. N. Baker,[2] and J. W. Gjerloev[4]

[1] Previous studies have shown the connection between electron precipitation and the excess amounts of nitric oxide at auroral latitudes. In this study the electron energy deposition derived from thermospheric nitric oxide (NO) measurements is compared with the electron energy deposition derived from X-ray bremsstrahlung measurements. The electron energy deposition is derived from nitric oxide densities by use of a photochemical model for nitric oxide and is referred to as the modeled energy deposition. The comparisons are made for the beginning of five geomagnetic storms in 1998: 21 March, 2 May, 14 June, 26 June, and 16 July. By using these quite different methods to derive the total electron energy deposition (4–100 keV), the results show that we have a generally good understanding of the physics and chemistry of the energy transfer from electron precipitation in the lower thermosphere. The comparisons also show some discrepancies. The modeled energy deposition is typically larger than the energy deposition derived from X-ray bremsstrahlung in the beginning of the storm period, whereas later on in the storm the energy deposition derived from X-ray measurements is largest. The cases where the modeled energy deposition is largest is probably due to production of NO occurring before the bremsstrahlung measurements. The systematic underestimate of the calculated energy deposition could be due to uncertainties in the reaction rates or in the characteristic electron energy used in the photochemical model. The effects from horizontal neutral wind on the NO gas from the production on the nightside to the observations on the dayside can also be a source of discrepancy.

**Citation:** Sætre, C., C. A. Barth, J. Stadsnes, N. Østgaard, S. M. Bailey, D. N. Baker, and J. W. Gjerloev (2006), Comparisons of electron energy deposition derived from observations of lower thermospheric nitric oxide and from X-ray bremsstrahlung measurements, *J. Geophys. Res.*, *111*, A04302, doi:10.1029/2005JA011391.

## 1. Introduction

[2] Nitric oxide is produced from the reaction between atomic nitrogen ($N(^4S, ^2D)$) and oxygen molecules. The ground state nitrogen ($N(^4S)$) will also cause destruction of NO; thus the increase in NO in the lower thermosphere is related to the relative amount of excited nitrogen atoms to ground state nitrogen ($N(^2D)/N(^4S)$) [*Barth*, 1992]. Energetic photoelectrons and precipitating electrons cause excitation and ionization in the upper atmosphere. The main sources of $N(^2D)$ are the results of dissociation of $N_2$ by energetic electrons, recombination of $NO^+$ and reaction of $N_2^+$ ions with atomic oxygen. It has been shown that the larger amounts of NO at higher latitudes are well correlated with the intensity of the auroral electron precipitation [e.g., *Siskind et al.*, 1989a; *Baker et al.*, 2001; *Petrinec et al.*, 2003; *Sætre et al.*, 2004].

[3] Owing to the rather long lifetime of NO (about 1 day at ~105 km altitude), the amounts produced during the night by auroral electrons will have time to rotate with the Earth toward the dayside without experiencing strong decay effects. The lower thermospheric neutral gas will be subject to neutral winds, and previous studies have shown evidence of an equatorward drift of the NO gas from the nightside to the dayside [*Barth et al.*, 2003; *Sætre et al.*, 2004].

[4] *Baker et al.* [2001] compared daily averages of the electron flux (E > 25 keV) measured by SAMPEX/LICA (Solar, Anomalous, and Magnetospheric Particle Explorer/ Low-Energy Ion Composition Analyzer) with daily averages of the NO density at 106 km altitude. The latter was observed by SNOE/UVS (Student Nitric Oxide Explorer/ Ultraviolet spectrometer), for three geomagnetic storm intervals in 1998. With a seasonal and latitudinal adjustment of the daily NO values, the linear relation between the two

---

[1]Department of Physics and Technology, University of Bergen, Bergen, Norway.
[2]Laboratory for Atmospheric and Space Physics, University of Colorado, Boulder, Colorado, USA.
[3]Geophysical Institute, University of Alaska Fairbanks, Fairbanks, Alaska, USA.
[4]Johns Hopkins University Applied Physics Laboratory, Laurel, Maryland, USA.

data sets had a correlation coefficient of 0.690. They also compared the daily NO density with the hemispherical power index (HPI) derived from NOAA (National Oceanic and Atmospheric Administration) measurements. The HPI is an estimate of the total incoming power into the upper atmosphere and is normally dominated by electrons with energy 1–10 keV. These comparisons gave a correlation coefficient of 0.629.

[5] The statistical analysis of *Petrinec et al.* [2003] compared three years (March 1998 through March 2001) of NO observations made by SNOE/UVS, with the daily averaged fluxes of X-ray bremsstrahlung measured by PIXIE (Polar Ionospheric X-ray Imaging Experiment) on board the Polar spacecraft. When the NO data from SNOE/UVS were delayed 1 day with respect to the PIXIE data, the correlation coefficients at the altitudes of maximum NO density (106–110 km) also were ~0.6.

[6] In a more detailed analysis, *Sætre et al.* [2004] compared the electron energy deposition derived from time-integrated X-ray fluxes measured by PIXIE and the NO density measured by SNOE/UVS for the beginning of a geomagnetic storm on 2 May 1998. The NO density observed by SNOE/UVS on the dayside was produced by electron precipitation the preceding night. The PIXIE measurements were integrated in geographical boxes for consecutively longer intervals of time, tracking all the energy input, from night to day, into the geographic areas beneath the separate SNOE orbits. The linear relationship between the NO density and the time-integrated energy deposition at 106 km altitude had a correlation coefficient of 0.91.

[7] *Cleary* [1986] compared NO densities as a function of altitude (105–125 km), measured by a rocket-borne spectrometer on 10 August 1982 launched at 0335 LT, with NO calculated from a one-dimensional photochemical model. The model was a prior version of the one used in this study. It included vertical diffusion of NO and $N(^4S)$ and calculated the photoelectron flux from the photoelectron model of *Strickland and Meier* [1982]. The branching ratios of $N(^4S)$ and $N(^2D)$ from the dissociation of $N_2$ from energetic electrons were 0.4 and 0.6, respectively [*Strickland and Meier*, 1982]. The photodissociation frequency of NO was $5.7 \times 10^{-6}\,s^{-1}$ [*Nicolet and Cieslik*, 1980]. The comparisons showed a good fit to the measured NO density, when the simulated aurora had a characteristic energy of 10 keV and continuous energy flux of 0.5 ergs $cm^{-2}\,s^{-1}$. The latitude, solar zenith angle, and local time used in the model were the same as those during the time of the rocket launch.

[8] *Siskind et al.* [1989a] calculated the NO density using a previous version of the time-dependent, one-dimensional photochemical model used here [*Bailey et al.*, 2002]. The HPI derived from NOAA 6 and 7 particle measurements specified the time history of the electron precipitation, with flux and characteristic electron energies updated every hour. The auroral particle precipitation pattern was derived from a statistical model. The calculated NO density was compared with NO measurements from SME (Solar Mesosphere Explorer), for the areas along the SME orbital track at higher latitudes. The comparisons were made for the auroral storm of 19 September 1984. The NCAR thermospheric general circulation model (TGCM) was used to calculate the response of the background neutral atmosphere. They saw an increase in both the modeled and the observed NO

density due to the storm. However, the magnitude and the amplitude of the storm increase of the modeled NO density, significantly exceeded the observed NO density. The overestimate was thought to be due to the yield of $N(^2D)$ of 60–70% from the dissociation of $N_2$ by energetic electrons being too large. Another explanation for the overestimate was that the vertical advection, which was not accounted for in the model, could be a significant loss mechanism of NO.

[9] *Bailey et al.* [2002] made a new version of the time-dependent, one-dimensional photochemical model for nitric oxide. The model calculates the NO density produced by photoelectrons and auroral electron precipitation. It includes calculations of the energetic electron energy deposition at each time step. The model assumes a continuous electron precipitation in the local time sector between 2100 and 2400, with a Maxwellian energy distribution with a characteristic energy of 4 keV. The electron energy flux is adjusted until the calculated NO density at 110 km altitude equals the NO-density measured by SNOE/UVS [*Solomon et al.*, 1996]. The model includes turbulent and diffusive transport of the NO gas but does not include horizontal transport of the neutral gas.

[10] In this study the electron energy deposition is derived from SNOE/UVS nitric oxide measurements by use of this photochemical model. This energy deposition is referred to as the modeled energy deposition. The electron energy deposition is also derived from X-ray bremsstrahlung measurements [*Østgaard et al.*, 2000] provided by the PIXIE camera on the Polar spacecraft [*Imhof et al.*, 1995]. This study compares the electron energy deposition derived from these two separate methods. The comparisons are made for the beginning of five geomagnetic storm time events in 1998 when Polar was at apogee approximately 9 $R_E$ above the Northern Hemisphere. PIXIE had a global view of the northern auroral oval for ~10 hours for each apogee pass.

[11] Four of the five events in this study have rather quiet geomagnetic conditions prior to the storm onset. When the results of the comparisons are interpreted, we use the AE index from the SuperMAG database [*Gjerloev et al.*, 2004] to consider the possible contribution from electron precipitation prior to the PIXIE observations.

## 2. Model Calculations and SNOE/UVS Measurements of NO

[12] The model used in this study is an improved version of a photochemical model [*Cleary*, 1986; *Siskind et al.*, 1989a, 1989b, 1990, 1995; *Barth*, 1992], with updated reaction rate coefficients and photoelectron flux calculations [*Bailey et al.*, 2002]. It is a time-dependent, one-dimensional model of nitric oxide that includes energetic electron transport, both for photoelectrons and auroral electrons. The model uses photochemical equilibrium to calculate the vertical profiles of NO, $N(^4S,^2D)$, and the ions $NO^+$, $O_2^+$, $N_2^+$, $O^+$, and $O^+(^2D)$. The photochemical model includes the vertical transport of NO and $N(^4S)$. The extreme ultraviolet solar flux (20–103 nm) is calculated using the model of *Hinteregger et al.* [1981], with the 10.7 cm solar radio flux as input parameter. The solar soft X-ray irradiance used in the model is measured directly by sensors on board the SNOE spacecraft [*Bailey et al.*, 2000]. The flux of the photoelectrons is calculated using the "glow" model of
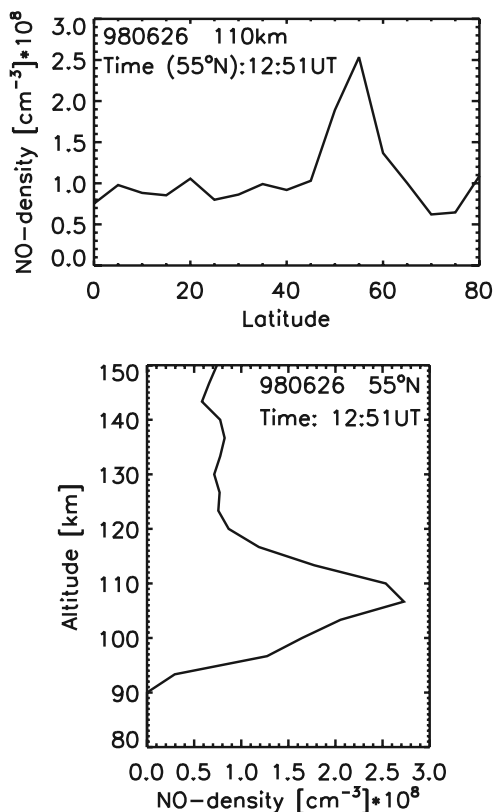
**Figure 1.** Nitric oxide density measured by SNOE 26 June 1998, 1251UT (at 55°N); (top) NO density at 110 km altitude as a function of geographic latitude and (bottom) NO density at 55°N as a function of altitude.

*Solomon et al.* [1988], where the electron transport algorithm is a two-stream code of *Banks and Nagy* [1970]. The model atmosphere used for the neutral constituents and for the temperature is the NRLMSISE-00 model [*Picone et al.*, 2002], where hourly values of the 10.7 cm flux and the Ap geomagnetic index are used as inputs.

[13] We use NO observations from SNOE/UVS as input to the model [*Barth et al.*, 2003]. SNOE had a Sun-synchronous orbit at 556 km altitude with the ascending node at 1030 LT. The nitric oxide density, as a function of altitude, was measured by limb observations of the fluorescence of NO molecules by solar radiation. Thus the observations were made only on the dayside of the orbit. Figure 1 shows an example of the NO density measured by SNOE 26 June 1998, 1251 UT (at 55°N), as a function of latitude and of altitude. The maximum NO density is at auroral latitudes and most often at 106–110 km altitude. The larger amounts of NO at higher latitudes have been produced by auroral electron precipitation during the night and then the NO gas rotated with the Earth over to the dayside where it was observed by SNOE/UVS. In the model, the areas beneath the SNOE orbit are assumed to have experienced 3 hours of precipitation in the local time sector from 2100 to 2400 LT during the preceding night. The precipitating electrons are set to a Maxwellian energy distribution with a 4 keV characteristic energy. The initial condition for the electron flux is $1\,\mathrm{mW\,m^{-2}}$ between 2100 and 2400 LT. The model results are compared with the nitric oxide density for each SNOE orbit at 110 km

altitude, for 5° latitude bins between 50°N and 70°N. The ratio between the observed and the calculated NO densities is used in a new estimate of the electron flux, and the model calculation is repeated until the electron flux gives a result that is consistent with the SNOE/UVS observations [*Barth et al.*, 2004]. The electron flux is multiplied with the 3 hours of precipitation time so that we have the total electron energy deposition per unit area independent of the actual length of the precipitation event. The calculations include the different loss processes of NO, some of which transform NO into other odd nitrogen species. Photodissociation of NO by solar far ultraviolet radiation gives the product of ground state nitrogen which will react with another NO molecule and produce molecular nitrogen and atomic oxygen. The effective lifetime of this reduction of NO is 19.6 hours [*Minschwaner and Siskind*, 1993; *Murray*, 1994; *Siskind*, 2000]. The photodissociation frequency at altitudes where the solar UV radiation is unattenuated is $7.34 \times 10^{-6}\,s^{-1}$. Two nitric oxide molecules are destroyed as a result of each photodissociation. This applies to solar-illuminated NO when there are no production processes or when NO is in equilibrium with production and loss mechanisms. At the equator, with daylight of 12 hours, the excess nitric oxide amount decreases to 54% of its initial value during a 24-hour period [*Barth and Bailey*, 2004]. The 35 reaction equations for the model are listed in Table 1 in the work of *Barth* [1992] and the updated reaction rates are listed in the appendix of *Bailey et al.* [2002] and also in the work of *Barth et al.* [1999]. The model does not include calculations of the horizontal transport of the NO gas due to neutral winds. In this study the latitude profiles of the total electron energy deposition are also compared so that possible meridional drift of the NO gas can be considered.

## 3. Electron Energy From X-Ray Bremsstrahlung Measurements

[14] The X-ray camera PIXIE on board the Polar satellite detects X-rays in the energy range of ~2–22 keV. When precipitating electrons are slowed down in the atmosphere by molecules and atoms, X-ray photons are emitted. The energies of the emitted X-rays are dependent on the energy of the precipitating electrons. The X-rays detected by PIXIE are divided into six energy bins to improve the statistics. Thus we find the energy spectrum of the X-ray bremsstrahlung. There is a known relation between the X-ray energy spectrum and the precipitating electron energy spectrum [*Berger and Seltzer*, 1972]. To obtain the electron energy spectrum from the PIXIE X-ray data, we use a look-up table based on an electron-photon transport code (developed from a neutron transport code [*Lorence*, 1992]). This look-up table gives values of the X-ray fluxes emitted at different zenith angles for different exponential electron energy spectra. This method determines the electron spectrum from 4 keV to 100 keV which yields an X-ray spectrum that best fits the observed photon spectrum. The electron energy flux can then be calculated by integrating the electrons from 4 to 100 keV. The same is done for the spectra from the photochemical model. The lower electron energy is set to 4 keV as PIXIE measures X-rays down to ~2 keV. The electron energy spectra from the PIXIE data are represented by single or double exponentials, depending on what best fits the measured X-rays. This method was described in more detail by *Østgaard et al.* [2000, 2001].

[15] In 1998 the Polar satellite had an apogee above the northern auroral oval at $\sim 9$ R$_E$. The PIXIE camera had a global view of the oval for almost 10 hours for each apogee pass. The PIXIE data have been organized in geographical boxes and the electron energy fluxes derived from these measurements have been integrated over time so that we get the total electron energy deposition over specific areas. These areas are the same as the ones beneath the SNOE orbits where the photochemical model calculates the necessary amount of electron energy deposition to produce the observed NO-density on the dayside.

## 4. Comparisons

[16] The five events compared in this study are at the beginning of geomagnetic storms for which the geomagnetic conditions have been rather quiet the preceding day. We tried to select events where the PIXIE measurements started before the onset of the storm. The AE, AL, and AU indices for the five events, and for the day prior to the storm, are plotted in Figure 2. The dashed lines show the time interval where PIXIE was making measurements. For 21 March there is evidence for some substorm activity the previous day, and there was strong activity starting $\sim 4$ hours before the PIXIE measurements. The NO density observed by SNOE may in part have been produced by electron precipitation in that time range. Thus the modeled energy deposition will tend to be larger than what we are able to derive from the PIXIE measurements for this day. The 2 May event had rather quiet conditions prior to the PIXIE measurements. For this case, we would expect the energy deposition derived from the bremsstrahlung spectra to be equal to the modeled energy deposition. For the July and June events there was some activity before the PIXIE measurements, however not as severe as for the March event. Thus we expect the modeled energy deposition to be rather similar to the energy deposition derived from PIXIE.

[17] Figure 3 shows the time-integrated X-ray bremsstrahlung intensity ($2-9$ keV) measured by PIXIE (white globe) and the NO density measured by SNOE/UVS (blue globe). The images are in geographic coordinates. The time intervals for the PIXIE measurements, and the times for the SNOE observations on the dayside are indicated under each plot. The PIXIE images are made from global images and show the accumulated X-ray intensity from the entire time interval. The NO images are made from several SNOE orbits since SNOE/UVS did not have a global view. If one moves clockwise from the dark blue sector into the colored sector, one first sees the NO density observed in the beginning of the time interval indicated under the plot. This NO density will correspond to the time-integrated X-rays for the same areas. When one continues to move clockwise, one comes to areas where the NO observations were made later in the SNOE time interval. The latest SNOE orbits may include NO density produced by electron precipitation that occurred after the PIXIE measurements. Thus the NO density from the latest SNOE orbits will correspond to more intense time-integrated X-ray bremsstrahlung than we are able to get from the time-limited PIXIE measurements. However, the images clearly show that both PIXIE and SNOE/UVS observed the results of energetic particle precipitation over the same large-scale areas. Whereas

PIXIE observed the effects immediately, SNOE observed the increase of the long-lived NO density later on when the precipitation areas had rotated with the Earth over to the dayside. In the images for 2 May 1998 we see that the maximum NO-density is south of the maximum time-integrated X-ray bremsstrahlung intensity. This could be due to horizontal transport of NO by neutral winds.

[18] The total electron energy deposition as a function of latitude (and longitude) is plotted in Figures 4a, 4b, 4c, and 4d for the 2 May, 14 June, 26 June, and 16 July 1998, respectively. The dashed line is the energy derived from nitric oxide observations and the solid line is the energy derived from the PIXIE bremsstrahlung measurements. The lower x-axis shows the geographic latitude of the area for which we are comparing, and the upper x-axis displays the longitude. The total energy deposition is given in keV/cm$^2$. The time written in each plot is the time of the SNOE observations (at 70°N). Except for the last two plots of 2 May and 26 June and the last plot of 16 July, this time is also the end of the interval for which the PIXIE data have been integrated. For these five particular cases, we assume that the production occurring on the morningside for the current areas after PIXIE stopped measuring is negligible compared to the previous nightside production. Thus we include these five orbits in our comparisons for better statistics. There is a generally good correspondence between the two data sets. However, at higher latitudes the modeled energy deposition sometimes tends to be very low compared to the energy deposition derived from PIXIE, whereas at lower latitudes it can even be larger than the PIXIE-derived energy deposition. This is quite often the case for the 21 March 1998 event (not shown), where there was activity prior to the PIXIE measurements. For 2 May, where the geomagnetic conditions were rather quiet before the PIXIE observations, the energy deposition derived from PIXIE was always larger than the modeled energy deposition. For the other three events, there could be electron precipitation before the PIXIE measurements, but not as severe as for the 21 March event. The modeled energy depositions for the June events and the 16 July event are sometimes a bit larger but the overall tendency is that the PIXIE derived energy deposition is largest.

[19] Figure 5 shows the total electron energy deposition, modeled and that derived from PIXIE, beneath the SNOE orbits for each of the five events. The energy deposition has been averaged over the latitude interval covered by the measurements. This comparison would not be as influenced by possible meridional wind effects. As time goes on, the amount of integrated energy deposition increases. In the beginning of the events the modeled energy deposition is typically larger than the energy deposition derived from PIXIE. This indicates that the SNOE NO observations include the energy deposited before PIXIE started measuring. As time goes on, the PIXIE derived energy deposition is larger by almost a factor of 2, except for the 21 March event. The total energy deposition derived from PIXIE gives the lower limit of the electron energy input due to the time limitations of the bremsstrahlung observations.

## 5. Discussion

[20] Our results show a generally good correspondence between the estimates of energy deposition in the Earth's
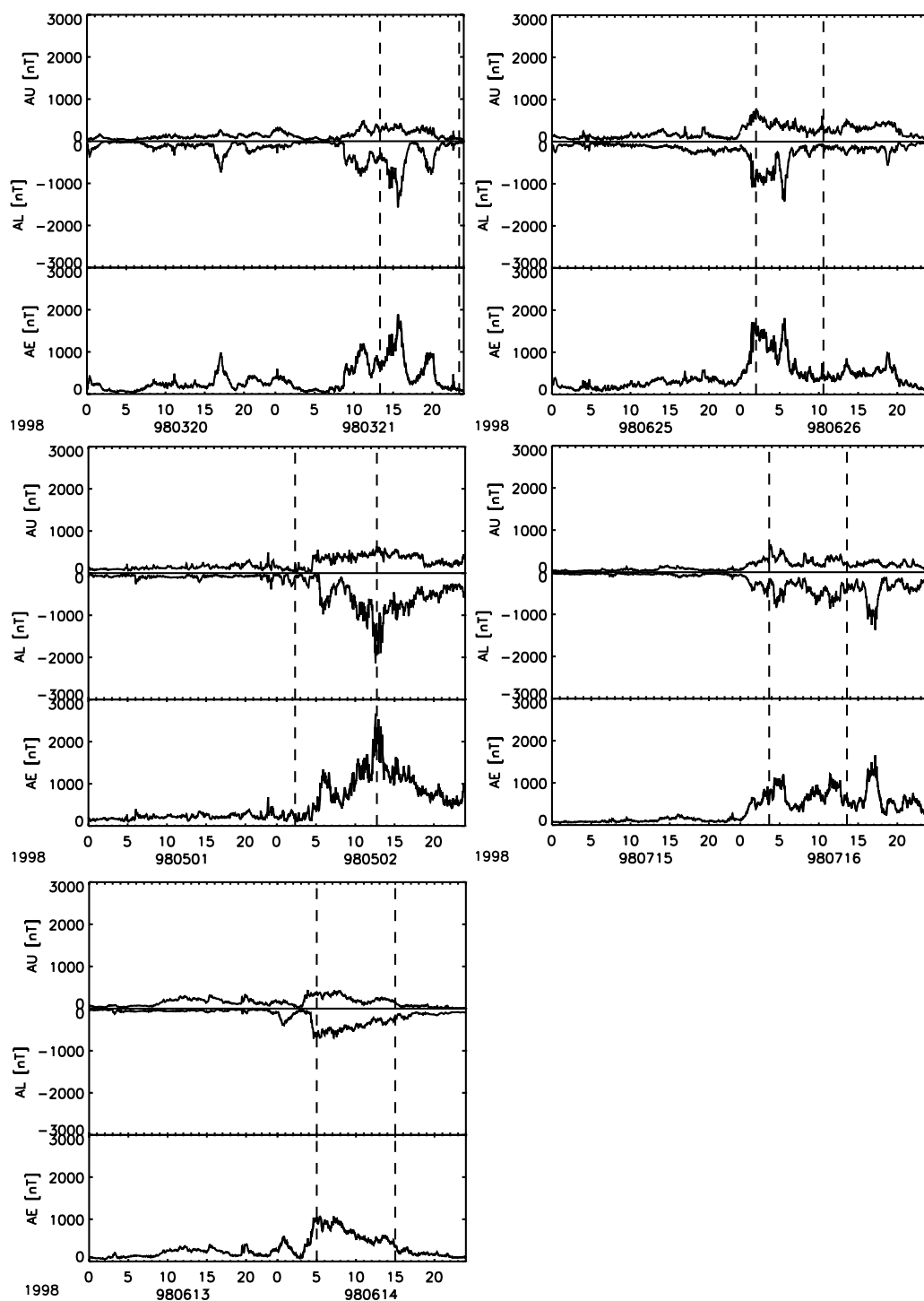
**Figure 2.** AU, AL, and AE index, from SuperMAG, for the five events investigated in this study and for the previous day. The dashed lines indicate the time interval of the PIXIE measurements.

auroral regions using two completely different methods. Given the success of such comparisons, this work gives us confidence that we have a good basic understanding of the physics and chemistry of electron precipitation and subsequent vertical transport in the lower thermosphere.

[21] Given the overall agreement, the comparisons nonetheless show evidence for a too low electron energy deposition derived from the nitric oxide measurements. One possible reason for this is that the assumption in the photochemical model of a Maxwellian characteristic energy of 4 keV, and hence the maximum NO density at 110 km altitude, is not always correct. The NO density can have its maximum at other altitudes, and in such cases, the NO density calculated from the photochemical model will be compared with an observed NO density at 110 km altitude which is lower than the maximum NO density. Thus the electron energy deposition necessary to produce the calculated NO density will be lower than actually was the case.
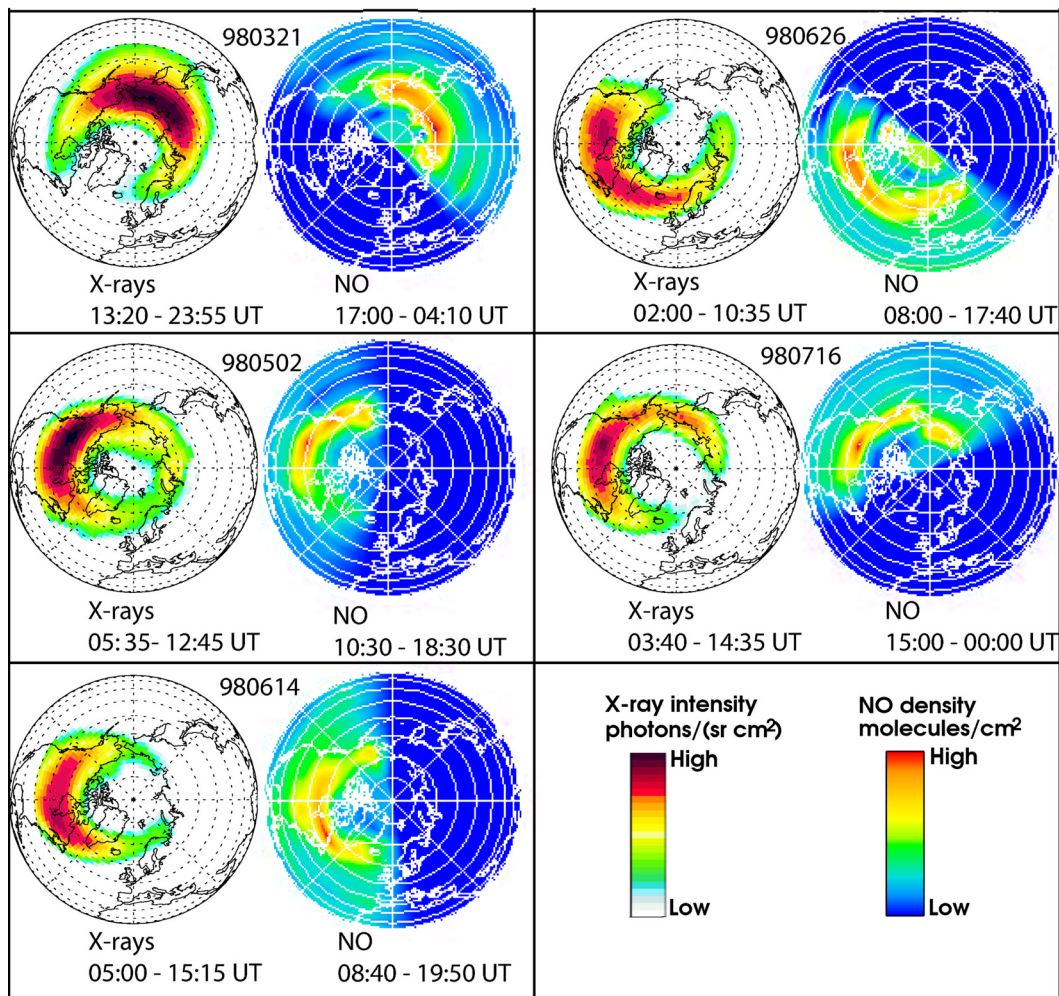
**Figure 3.** Time-integrated X-ray bremsstrahlung ($\sim 2-9$ keV) from PIXIE measurements (white globe) in photons/(sr cm$^2$), and nitric oxide density at 110 km altitude measured by SNOE/UVS (blue globe) in molecules/cm$^2$. The images are in geographic coordinates. The time range for developing each plot is written beneath each image. If one moves from the dark blue sector into the colored sector, the first part of the SNOE image will correspond to the PIXIE observations for the same areas, whereas the last part might contain NO densities produced after PIXIE stopped measuring.

Two altitude profiles of the NO density for the 26 June 1998 event, measured by SNOE/UVS, are shown in Figure 6. The ratios between the maximum NO density and the density at 110 km altitude are also given for the two altitude profiles. Sometimes this ratio can be quite large, as for 55°N (see also Figure 4c, middle right). However, this effect can not explain all the cases where the modeled electron energy is very low compared to the PIXIE-derived energy deposition (e.g., the 60°N case, see Figure 4c bottom right). Considering the fact that SNOE/UVS would also measure NO densities produced before the beginning of the PIXIE measurements, the modeled electron energy should not be lower than that derived from the X-ray bremsstrahlung measured for a limited time interval.

[22] The uncertainty in the nitric oxide density determined from SNOE/UVS observations is discussed by *Barth and Bailey* [2004]. The uncertainty in the instrument calibration is 14%, the uncertainty in the solar flux at 237 nm is 7%, and the uncertainty in the molecular parameters used to determine the nitric oxide fluorescence is 10%, giving a combined uncertainty of about 20%. The uncertainty in the X-ray bremsstrahlung determined from PIXIE measurements is low in this study. Since we accumulate the photon intensity over long time intervals, the number of counts are quite high, and thus the PIXIE measurement uncertainties are considered to be negligible compared to the uncertainty in deriving the energy spectra. The look up table based on the Lorence code gives the X-ray flux versus zenith angle for different electron spectra. In the very beginning of the events PIXIE had a more slant viewing, and the uncertainty in the X-ray flux derived from the look up table is $\sim 10\%$. Further on in the observation period the zenith angles are not so large ($<40° \pm 7°$), and the uncertainty in the X-ray flux from the table is less than 5%. This uncertainty should not result in significant systematic errors. The actual fitting of the energy spectra to the PIXIE measurements is the main uncertainty when deriving the energy deposition from the X-ray bremsstrahlung. Considering that we use several spectra when deriving the energy deposition and the fact that we integrate only over energies where PIXIE gives
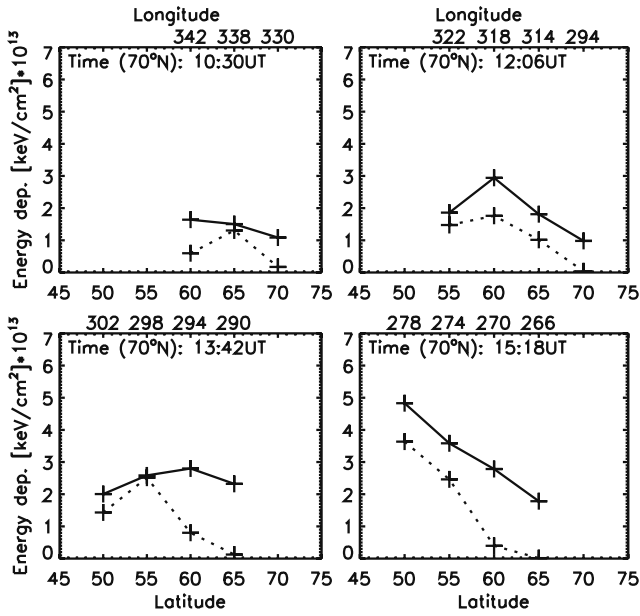
**Figure 4a.** Total electron energy deposition for 2 May 1998 derived from SNOE nitric oxide observations (dashed line) and derived from PIXIE measurements (solid line). The latitude and longitude for the areas we are comparing are written on the lower and upper x-axis.
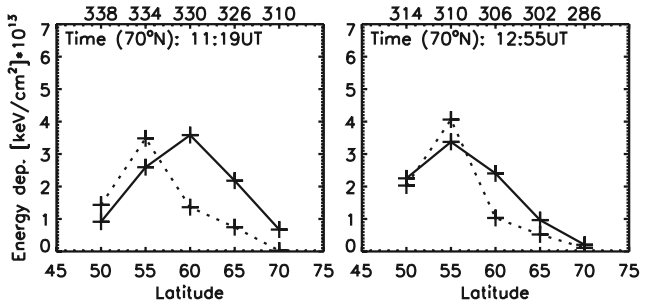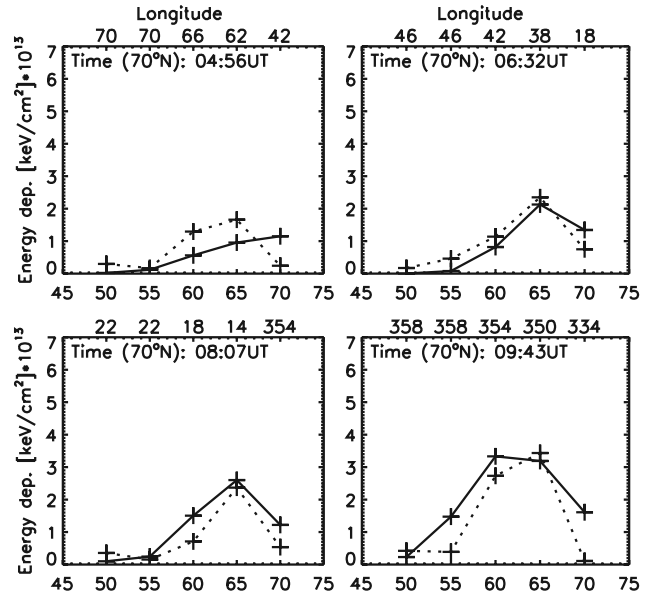
**Figure 4c.** Same as for Figure 4a but for 26 June 1998.

reliable information (4–100 keV), the uncertainty of the fitting of the spectra is less than 25%. The uncertainties in the method of deriving electron energy deposition from X-ray bremsstrahlung measurements are far from a factor of two and are not systematic.
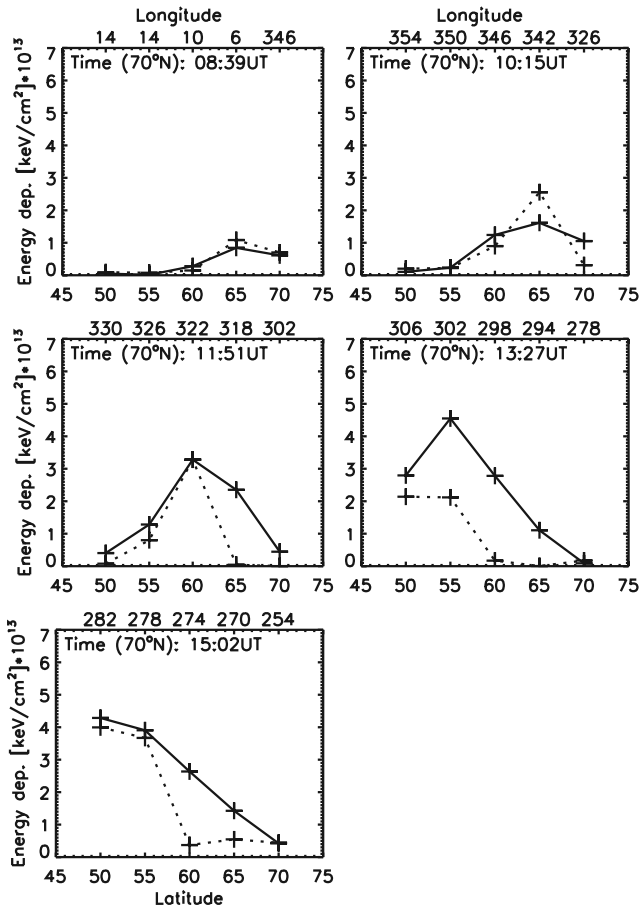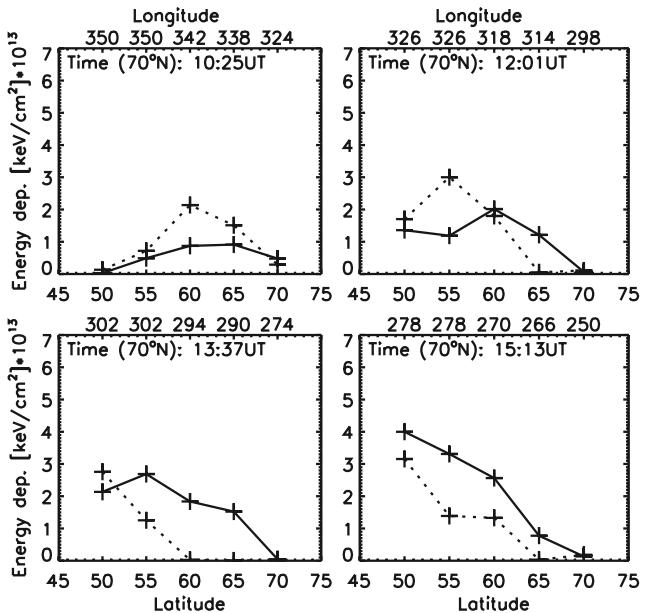
**Figure 4b.** Same as for Figure 4a but for 14 June 1998.

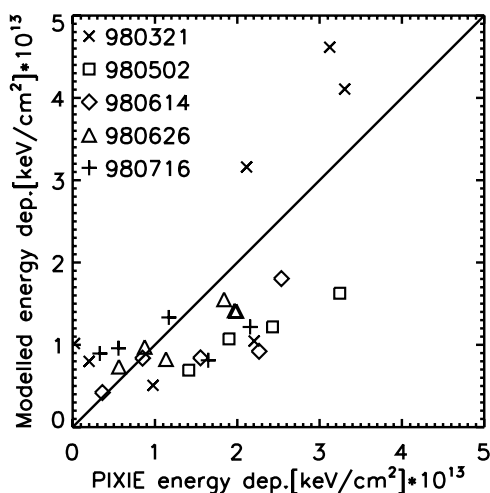**Figure 4d.** Same as for Figure 4a but for 16 July 1998.

**Figure 5.** The total electron energy deposition (4–100 keV) underneath the SNOE orbits, averaged over the latitude interval covered by the measurements.

[23] Another source of discrepancy may be the effects of horizontal transport of the NO gas from north to south. For some of the cases, i.e., the last two plots in Figure 4c, the modeled profile seems to be displaced equatorward relative to the PIXIE energy profile. This could be the effect of horizontal neutral winds. When modeling the energy input into the atmosphere from particle precipitation by use of photochemistry, the inclusion of neutral wind parameters would be helpful if only just to clarify the extent to which the discrepancies are due to meridional transport of NO.

[24] Another possible source of error may be that the calculations of NO density from electron precipitation are strongly dependent on the branching ratios for $N(^4S)$ and $N(^2D)$, especially from the dissociative recombination of ionized nitric oxide [*Barth et al.*, 1999]. The branching ratio for this reaction has been measured very precisely in the laboratory [*Vejby-Christensen et al.*, 1998] and found to be 0.85 for $N(^2D)$ with an uncertainty of 7%. A sensitivity test was conducted with the nitric oxide photochemical model using the extremes of branching ratio measurement. The result was a variation of 20% in the nitric oxide density calculated by the model.

[25] A last source of error could result from the loss of NO due to photodissociation from sunrise to the SNOE measurements at $\sim$1030 LT. The ultraviolet solar flux involved in the photodissociation of nitric oxide has an uncertainty of 7% and the uncertainty in the molecular parameters is estimated to be 14%, giving a combined uncertainty for the photodissociation rate of 16%. A sensitivity test was performed for a photodissociation rate 16% larger and 16% smaller than $7.34 \cdot 10^{-6}$ s$^{-1}$. The result was that the nitric oxide density had a decrease of 11% for the larger value and an increase of 16% for the smaller value.

[26] The combined uncertainty of the energy deposition derived from the SNOE observations is $\sim$30%. This includes the observation uncertainties ($\sim$20%), the variation of NO (20%) from branching ratio uncertainty in the recombination of NO$^+$, and the variation of NO ($\leq$16%) from the uncertainty in the photodissociation rate of NO.

The combined uncertainty of the energy deposition derived from the PIXIE measurements is 25–30%. This includes a maximum uncertainty in the X-ray flux from the Lorence's code (10%), the uncertainty of the fitting of the energy spectra (25%), and the uncertainty of the X-ray measurements ($\leq$5%).

[27] At latitudes below 60°N many of the discrepancies could be explained by the combined effects of these uncertainties. In the cases where the discrepancies are largest, most often at the highest latitudes, the combined uncertainties (25–30% for PIXIE and $\sim$30% for SNOE) are not sufficient to explain the lower-energy deposition modeled from the NO measurements. It is difficult to say at this point whether possible meridional transport of NO could explain these differences at the highest latitudes. We do not believe it is likely that the energy deposition derived from the PIXIE measurements is systematically overestimated. In some cases the modeled energy deposition is underestimated when the maximum NO density is not located at 110 km altitude, as assumed. However, at this point we are not able to explain most of the discrepancies at the latitudes over 60°N. For the cases where the energy deposition derived from SNOE is larger than that derived from PIXIE, the uncertainty
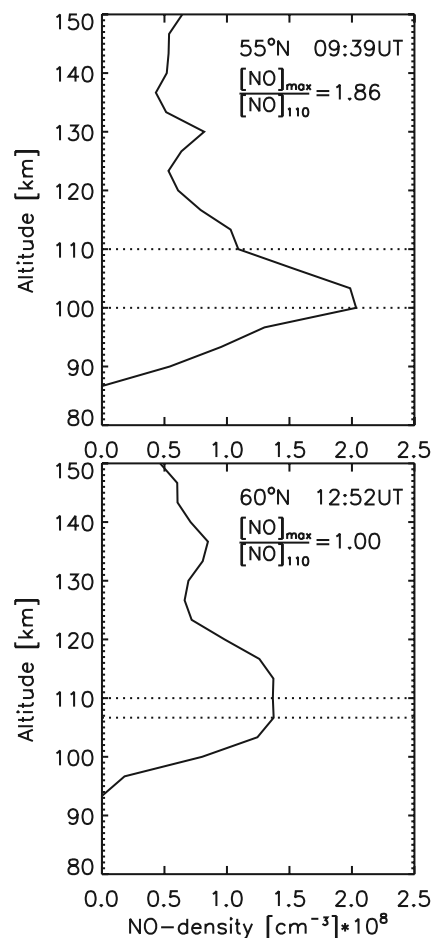


**Figure 6.** Two examples of the NO density measured by SNOE on 26 June 1998, with the ratio between the maximum NO value and the NO density at 110 km altitude.

of the precipitation prior to the PIXIE measurements will be significant.

## 6. Summary and Conclusion

[28] In this study we have compared the total electron energy deposition derived from nitric oxide measurements with use of a photochemical model and derived from X-ray bremsstrahlung measurements. The comparisons are made for the beginning of five geomagnetic storms in 1998 where the activity was rather low the preceding day. In the photochemical model calculations, the electron energy was adjusted until the calculated NO density equaled the density measured by SNOE/UVS on the dayside. Thus the modeled electron energy deposition represents the total energy necessary to produce the excess amounts of NO in the lower thermosphere. The energy deposition derived from the PIXIE X-ray data is naturally limited to the time interval in which PIXIE was measuring. If there is precipitation before the PIXIE observations, this will be included in the modeled energy deposition but not in the PIXIE data. The total electron energy deposition derived from PIXIE observations can be considered as a lower limit. We found that the modeled energy deposition is systematically underestimated compared to the energy derived from the PIXIE measurements at the highest latitudes (typically $\geq 60°N$) and that the PIXIE and SNOE energy depositions are comparable within the range of the uncertainties at the lower latitudes ($<60°N$). The differences can in part be due to a possible southward drift of the NO gas and thus a displacement of the energy profiles. In some of the cases the assumptions made in the model calculations, with a characteristic Maxwellian energy of 4 keV and a maximum NO density at 110 km altitude, were not correct. The NO measurements would then have a maximum at a different altitude, and the electron energy deposition would be underestimated. The chemical reaction rates used in the photochemical model may also cause a systematic underestimate of the energy deposition.

[29] The results of this study give us nonetheless confidence that we have a good basic understanding of the physics and chemistry of the electron energy deposition and transport in the lower thermosphere. We believe that the minor adjustments that are necessary for improving the photochemical model can be done using the results of these comparisons with the PIXIE X-ray measurements.

## References

Bailey, S. M., T. N. Woods, C. A. Barth, S. C. Solomon, L. R. Canfield, and R. Korde (2000), Measurements of the solar soft x-ray irradiance by the Student Nitric Oxide Explorer: First analysis and underflight calibrations, *J. Geophys. Res.*, *105*, 27,179.

Bailey, S. M., C. A. Barth, and S. C. Solomon (2002), A model of nitric oxide in the lower thermosphere, *J. Geophys. Res.*, *107*(A8), 1205, doi:10.1029/2001JA000258.

Baker, D. N., C. A. Barth, K. E. Mankoff, S. G. Kanekal, S. M. Bailey, G. M. Mason, and J. E. Mazur (2001), Relationships between precipitating auroral zone electrons and lower thermospheric nitric oxide densities: 1998–2000, *J. Geophys. Res.*, *106*, 24,465.

Banks, P. M., and A. F. Nagy (1970), Concerning the influence of elastic scattering upon photoelectron transport and escape, *J. Geophys. Res.*, *75*, 1902.

Barth, C. (1992), Nitric oxide in the lower thermosphere, *Planet. Space Sci.*, *40*, 315.

Barth, C. A., and S. M. Bailey (2004), Comparison of a thermospheric photochemical model with Student Nitric Oxide Explorer (SNOE) observations of nitric oxide, *J. Geophys. Res.*, *109*, A03304, doi:10.1029/2003JA010227.

Barth, C. A., S. M. Bailey, and S. C. Solomon (1999), Solar-terrestrial coupling: Solar soft x-rays and thermospheric nitric oxide, *Geophys. Res. Lett.*, *26*, 1251.

Barth, C. A., K. D. Mankoff, S. M. Bailey, and S. C. Solomon (2003), Global observations of nitric oxide in the thermosphere, *J. Geophys. Res.*, *108*(A1), 1027, doi:10.1029/2002JA009458.

Barth, C. A., D. N. Baker, and S. M. Bailey (2004), Seasonal variation of auroral electron precipitation, *Geophys. Res. Lett.*, *31*, L04809, doi:10.1029/2003GL018892.

Berger, M. J., and S. Seltzer (1972), Bremsstrahlung in the atmosphere, *J. Atmos. Terr. Phys.*, *34*, 85.

Cleary, R. J. (1986), Daytime high-latitude rocket observations of the NO $\gamma$, $\delta$ and $\varepsilon$ bands, *J. Geophys. Res.*, *91*, 11,337.

Gjerloev, J. W., M. Friel, R. A. Hoffman, K. Takahashi, R. Barnes, C. Meng, and R. A. Greenwald (2004), The global magnetometer network initiative: SuperMAG, *Eos Trans. AGU*, *85*(47), Fall Meet. Suppl., Abstract SH41A-1079.

Hinteregger, H. E., K. Fukui, and B. R. Gilson (1981), Observational, reference, and model data on solar EUV, from measurements on AE-E, *Geophys. Res. Lett.*, *8*, 1147.

Imhof, W. L., et al. (1995), The Polar Ionospheric X-ray Imaging Experiment (PIXIE), *Space Sci. Rev.*, *71*, 385.

Lorence, L. J. (1992), CEPAS/ONELD version 2.0: A discrete ordinates code package for general one-dimensional coupled electron-photon transport, *IEEE Trans. Nucl. Sci.*, *39*(4), 1031.

Minschwaner, K., and D. E. Siskind (1993), A new calculation of nitric oxide photolysis in the stratosphere, mesosphere, and lower thermosphere, *J. Geophys. Res.*, *98*, 20,401.

Murray, J. E. (1994), Vacuum ultraviolet Fourier transform spectroscopy of the delta (0,0) and beta (7,0) bands of NO, *J. Chem. Phys.*, *101*, 62.

Nicolet, M., and S. Cieslik (1980), The photodissociation of nitric oxide in the mesosphere and stratosphere, *Planet. Space Sci.*, *28*, 105.

Østgaard, N., J. Stadsnes, J. Bjordal, R. R. Vondrak, S. A. Cummer, D. L. Chenette, M. Schulz, and J. G. Pronko (2000), Cause of the localized maximum of x-ray emission in the morning sector: A comparison with electron measurements, *J. Geophys. Res.*, *105*, 20,869.

Østgaard, N., J. Stadsnes, J. Bjordal, G. A. Germany, R. R. Vondrak, G. K. Parks, S. A. Cummer, D. L. Chenette, and J. G. Pronko (2001), Auroral electron distributions derived from combined UV and X-ray emissions, *J. Geophys. Res.*, *106*, 26,081.

Petrinec, S. M., W. L. Imhof, C. A. Barth, K. D. Mankoff, D. N. Baker, and J. G. Luhmann (2003), Comparison of thermospheric high-latitude nitric oxide observations from SNOE and global auroral X-ray bremsstrahlung observations from PIXIE, *J. Geophys. Res.*, *108*(A3), 1123, doi:10.1029/2002JA009451.

Picone, J. M., A. E. Hedin, D. P. Drob, and A. C. Aikin (2002), NRLMSISE-00 empirical model of the atmosphere: Statistical comparisons and scientific issues, *J. Geophys. Res.*, *107*(A12), 1468, doi:10.1029/2002JA009430.

Sætre, C., J. Stadsnes, H. Nesse, A. Aksnes, S. M. Petrinec, C. A. Barth, D. N. Baker, R. R. Vondrak, and N. Østgaard (2004), Energetic electron precipitation and the NO abundance in the upper atmosphere: A direct comparison during a geomagnetic storm, *J. Geophys. Res.*, *109*, A09302, doi:10.1029/2004JA010485.

Siskind, D. E. (2000), On the coupling between middle and upper atmosphere odd nitrogen, in *Atmospheric Science Across the Stratopause*, *Geophys. Monogr. Ser.*, vol. 123, edited by D. E. Siskind, S. D. Eckermann, and M. E. Summers, pp. 101–116, AGU, Washington, D. C.

Siskind, D. E., C. A. Barth, D. S. Evans, and R. G. Roble (1989a), The response of thermospheric nitric oxide to an auroral storm: 2. Auroral latitudes, *J. Geophys. Res.*, *94*, 16,899.

Siskind, D. E., C. A. Barth, and R. G. Roble (1989b), The response of thermospheric nitric oxide to an auroral storm: 1. Low and middle latitudes, *J. Geophys. Res.*, *94*, 16,885.

Siskind, D. E., C. A. Barth, and D. D. Cleary (1990), The possible effect of solar soft X rays on thermospheric nitric oxide, *J. Geophys. Res.*, *95*, 4311.

Siskind, D. E., D. J. Strickland, R. R. Meier, T. Majeed, and F. G. Eparvier (1995), On the relationship between the solar soft X-ray flux and thermospheric nitric oxide: An update with an improved photoelectron model, *J. Geophys. Res.*, *100*, 19,687.

Solomon, S. C., P. B. Hays, and V. J. Abreu (1988), The auroral 6300 Å emission: Observations and modeling, *J. Geophys. Res.*, *93*, 9867.

Solomon, S. C., C. A. Barth, M. J. Erikson, R. A. Kohnert, and A. W. Merkel (1996), The Student Nitric Oxide Explorer, *Proc. SPIE*, *2810*, 121.

Strickland, D. J., and R. R. Meier (1982), A photoelectron model for the rapid computation of atmospheric excitation rates, *NRL Memo. Rep.*, *5004*, 1–40.

Vejby-Christensen, L., D. Kella, H. B. Pedersen, and L. H. Andersen (1998), Dissociative recombination of $NO^+$, *Phys. Rev. A*, *57*, 3627.

————————————

S. M. Bailey, Geophysical Institute, University of Alaska Fairbanks, Fairbanks, AK 99775-7320, USA.

C. A. Barth and D. N. Baker, Laboratory for Atmospheric and Space Physics, University of Colorado, Boulder, CO 80303-7814, USA.

J. W. Gjerloev, Johns Hopkins University Applied Physics Laboratory, Laurel, MD 20723-6099, USA.

N. Østgaard, C. Sætre, and J. Stadsnes, Department of Physics and Technology, University of Bergen, Allégaten 55, N-5007 Bergen, Norway. (camilla.satre@ift.uib.no)